A machine learning based approach to clinopyroxene thermobarometry: model optimisation and distribution for use in Earth Sciences

C. Jorgenson[1*], O. Higgins[1], M. Petrelli[2], F. Bégué[1], and L. Caricchi [1]

[1]Department of Earth Sciences, University of Geneva, Geneva, Switzerland

[2]Department of Physics and Geology, University of Perugia, Perugia, Italy

* Corin Jorgenson (corin.jorgenson@unige.ch, ORCID iD: 0000-0002-0088-6062)

THE FOLLOWING MANUSCRIPT IS A NON-PEER REVIEWED PREPRINT SUBMITTED TO **EarthArXiv**. THIS ARTICLE IS CURRENTLY IN PREPARATION FOR SUBMISSION TO **Journal of Geophysical Research - Solid Earth**

Social media: @corinjorgenson @MAGEvolcano @4ohiggins4 @LucaCaricchi

Key Points:

- Machine learning random forest
- Clinopyroxene thermobarometry
- Model optimization

Abstract

Thermobarometry is a fundamental tool to quantitatively interrogate magma plumbing systems and broaden our appreciation of volcanic processes. Developments in random forest-based machine learning lend themselves to a more data-driven approach to clinopyroxene thermobarometry. This can include allowing users to access and filter large experimental datasets that can be tailored to individual applications in Earth Sciences. Here we present a methodological assessment of random forest thermobarometry, using the R freeware package "`extraTrees`", by investigating the model performance, tuning hyperparameters, and evaluating different methods for calculating uncertainties. We determine that deviating from the default hyperparameters used in the "`extraTrees`" package results in little difference in overall model performance (<0.2 kbar and <3 ºC difference in mean SEE). However, accuracy is greatly affected by how the final pressure or temperature (PT) value from the voting distribution of trees in the random forest is selected (mean, median or mode). This thus far has been unapproached in machine learning thermobarometry. Using the mean value leads to a higher residual between experimental and predicted PT, whereas using median values produces smaller residuals. Additionally, this work provides two comprehensive R scripts for users to apply the random forest methodology to natural datasets. The first script permits modification and filtering of the model calibration dataset. The second script contains pre-made models in which users can rapidly input their data to recover pressure and temperature estimates. These scripts are open source and can be accessed at https://github.com/corinjorgenson/RandomForest-cpx-thermobarometer.

Plain Language Summary

Determining the structure of magmatic plumbing systems is an integral part of understanding the processes preceding volcanic eruptions. Thermobarometry estimates the pressure and temperature of crystallisation of minerals that crystallise from the magma using their chemical composition. This can provide quantitative information on the depth and temperature of magma storage before eruption. Clinopyroxene, a common phenocryst found in volcanic rocks, has been shown to be a reliable mineral for thermobarometry. Classic thermobarometers use a single equation for a specific melt chemistry and are often rigid in their usage. There exists an alternative methodology which utilizes a machine learning

algorithm called random forest. This algorithm creates hundreds of hierarchical flowcharts called decision trees to generate predictive models which can be applied to natural data. Here we present a study which focuses on optimization of these models and presents users with two versions which they can access, modify, and use for their data. These two versions are available freely at https://github.com/corinjorgenson/RandomForest-cpx-thermobarometer and can be easily used within the freeware package R.

1. Introduction

Quantifying the pressure and temperature of mineral crystallization is an invaluable method to view the magmatic plumbing system of volcanoes, and constrain fundamental processes within the Earth's crust and mantle (Giacomoni et al., 2016; Ridolfi et al., 2008; Shane & Smith, 2013; Shaw, 2018; Smith, 2013). Clinopyroxene chemistry has been widely used for this endeavour by calibrating thermobarometers (Masotta et al., 2013; Neave & Putirka, 2017; K. D. Putirka, 2008). Classically these thermobarometers result in a single equation which links site-specific mineral chemistry (plus or minus equilibrium liquid data) to the variation in pressure or temperature of crystallisation. However, these formulas are often associated with large standard error estimates (SEE) and are only appropriate for specific melt compositions (e.g. Neave & Putirka, 2017 for ultramafic to intermediate compositions; Masotta et al., 2013 for alkaline magmas). Additionally, early thermobarometers are self-validated, which means that data used to regress the model are also used to validate it. This typically leads to data overfitting and an underestimated SEE (Nimis & Taylor, 2000; K. D. Putirka, 2008). Recent developments in machine learning applications to petrology by Petrelli et al., 2020 and Higgins et al., 2021 have resulted in a machine learning derived random forest approach to thermobarometry.

Random forest is a machine learning method that employs decision trees to populate an improved prediction-based model, using the results from a distribution of hundreds of trees to generate an output (Breiman, 2001, 2002; Ho, 1995). A decision tree is a hierarchical flowchart that determines an outcome when given a set of input variables (Figure 1). Each tree is comprised of branches and leaves, where the branches represent different pathways from the root to the desired outcome (the leaves). Branches split at nodes, where at each node a branch may spilt either left or right in the simplest case. When a

branch can no longer split, a leaf is "grown", and the desired output is reported. In our case the branches and nodes are dictated by clinopyroxene geochemistry, and the leaves are pressure (P) or temperature (T) of crystallization. However, the chemical element (or oxide) selected at each node greatly influences the predictive outcome of the tree. Hence the random forest model is ultimately comprised of hundreds of decision trees. Therefore, from these hundreds of decision trees, the output (predicted P or T) is the mean value from all decision trees in the case of regressive models. To allow the model to construct reasonable decision trees for prediction of natural data we input a dataset of experimentally derived clinopyroxenes (e.g., Supplementary Figure. 1) with a known pressure and temperature of crystallization, hereafter referred to as the calibration dataset. In principle the idea is very simple – the algorithm uses the calibration dataset to create a predictive model, which we can apply to natural samples. However, there are several parameters to consider when producing a model for reliable prediction of natural data, in addition to several statistical metrics for selecting the best estimation from the voting distribution of decision trees (e.g., mean, median, or mode).

Increasingly models and methodologies for Earth science applications have moved to powerful and adaptable codes for programs such as R, python, and MATLAB as well as hosted on online servers such as github (Georgeais et al., 2021; Ghiorso & Wolf, 2019; Iacovino et al., 2020; Lemenkova, 2019; Lubbers et al., 2019). This allows for more user interaction and, in some cases, provides open-source options to users regardless of their operating system or access to apps like excel. Thus, the twofold aim of this work is to 1) build and test the performance of a thermobarometer model for clinopyroxenes and 2) provide a comprehensive explanation of how to apply our thermobarometer for applications to natural data. Our regression strategy offers a generalised model that can be tailored for certain settings, applications, or other suitable mineral phases (e.g., amphibole; Higgins et al., 2021).

2. Methods

2.1. Datasets and Preprocessing

The calibration dataset is comprised of experimentally grown clinopyroxenes and equilibrium liquids compiled from the Library of Experimental Petrology Research database and additional works not included in the LEPR database (Hirschmann et al., 2008; Supplementary Table 1). The unfiltered

calibration dataset features 1773 datapoints, including temperatures from 679 – 2180 ºC, 0 - 160 kbar and 6.5 – 78.18 wt.% SiO_2. All clinopyroxene data were first filtered for reasonable cations within a range from 3.96 – 4.04 as suggested by Ziberna et al., (2016). The calibration dataset was further filtered based on $Kd_{Fe\text{-}Mg}$ (Klügel & Klein, 2006). Following Putirka (2008) we accepted a range of $Kd_{Fe\text{-}Mg}$ = 0.04 – 0.68 (Figure 2A). Then the data was filtered to remove the high-pressure experiments (> 50 kbar) which are not in great numbers. Finally, any data points with abnormally low SiO_2 liquid contents (< 35 wt. % SiO_2) were removed. This forms the final calibration dataset (Supplementary Table 1, Supplementary Figure 1).

Typically, classic thermobarometers are calibrated and tested in the following way. Firstly, a large (>80 % of total experiments) training dataset is selected from the total calibration dataset of experiments. This dataset is used to calibrate with the chosen regression strategy (e.g., linear regression, multivariate linear regression). The remaining data are placed into a test dataset which is used to assess the performance of the model. This is commonly achieved by running each composition in the test dataset through the regressed model and calculating the standard error estimate or distribution of residual values to the known experimental values (K. D. Putirka, 2008; Ridolfi et al., 2008).

The pressure-temperature distribution of the calibration dataset is not uniform – experiments are preferentially run at low pressures. Thus, randomly extracting from the calibration dataset unevenly weights the test set to have low pressure experiments, resulting in a poor representation of the SEE. To circumvent this issue our test dataset was uniformly extracted from the calibration dataset on a gridded basis (Supplementary Figure 1b). Sampling from a gridded distribution offers additional biases as in oversampling PT grid spaces that may have a small distribution of data – thus the grid spacing was randomized for each 200 runs and samples were not extracted if the grid space did not have at least two datapoints. This results in each test dataset sampling approximately a tenth of the total calibration dataset. Once the respective test and train data sets are extracted then the model is run for each set (200 times). By generating multiple random splits of test and train datasets we can evaluate the full effect of sampling on the SEE (and other model performance metrics). This effect is not considered in conventional calibration methods (e.g. Ridolfi et al., 2010; Ridolfi & Renzulli, 2012).

2.2. Components of a random forest

We chose to use the R package "extraTrees" developed by Simm et al., (2014) although the "randomForest" package by Breiman (2002) produces comparable results at greater computational expense (Petrelli et al., 2020). Within the "extraTrees" package exist several parameters that can affect model performance. Firstly, ntree (default = 500) determines the number of individual decision trees which are used for prediction. A sufficiently high number of trees must be used to provide stability of the variable importance. Generally speaking more trees give better results at the cost of processing time, although this is dependent on the dataset used (Breiman, 2001; Probst et al., 2019; Probst & Boulesteix, 2018). Secondly, mtry, dictates how many variables (in our case, the major element chemical constituents of clinopyroxene) are considered at each node. The mtry is more influential on the overall performance of the model and default mtry for "extraTrees" is the total number of variables divided by three (Probst et al., 2019; Simm et al., 2014). For each node in a decision tree, a random subset of variables equal to mtry are selected from which the best performing variable is eventually chosen. In "extraTrees" each node is split at a random value, as described Simm et al., (2014). To choose which of the selected variables is used for the next node, a score is calculated for each variable for regressive models. This score is calculated considering a proportional negative variance for each split (denoted by L for left and R for right).

$$score = n_L * var_L + n_R * var_R \quad (1)$$

$$var = -\frac{1}{n}\sum_{i=1}^{n}\left(y_i - mean(y)\right)^2 \quad (2)$$

Where n_L and n_R are the number of datapoints assigned to each left or right branch, and var is the negative variance of the data on the left (or right) side of the split for the y variables (Simm et al., 2014). The tested variable with the highest score is chosen for the node.

The "extraTrees" package provides an additional variable for modification which is the number of random cuts (numRandomCuts). The package "extraTrees" may provide more than two splits to allow for non-binary splitting. This can be envisioned in real life by a tree splitting a branch

153 in three sections instead of two. As noted in the "`extraTrees`" vignette, optimization may occur
154 when using `numRandomCuts` between 3 – 5.

155 Each tree generates a single output value and thus a forest with 300 trees generates 300 pressure or
156 temperature estimates. In order to choose the best estimate, the random forest takes the mean or modal
157 value for regression or classification models respectively. Though our models are regressive, and thus
158 the default is to use a mean estimation, we additionally calculate the median and modal estimates to
159 evaluate the model performance. The median is calculated by taking the middle value from a sorted set
160 of values. Thus, to avoid the rare case where there is an even number of trees, and the two center points
161 are drastically different, we have decided to use an odd number of trees to average the two values.

162 2.3. Error assessment

163 Before continuing, we must consider the argument of accuracy versus precision. Random forest is
164 effective at generating precise values, but a reliable thermobarometer needs to be accurate as well as
165 precise. As such, the evaluation of the uncertainty of an individual model will be led by the R^2 values
166 (equation 3, where RSS is the residual sum of squares and TSS is the total sum of squares) and the
167 residual values (absolute difference between the experimental temperature or pressure and the
168 temperature or pressure output from the model), in addition to the standard error estimate (SEE) and
169 the interquartile range (IQR) of the voting distribution.

170 $$R^2 = 1 - \frac{RSS}{TSS} \quad (3)$$

171 To avoid self-validation and overfitting, the test dataset must not be used in the training dataset
172 which trains the model. Varying the test dataset is one the largest sources of variation in the SEE and
173 so we have decided to extract the test dataset and running of the model 200 times. Then the average
174 SEE is taken from the distribution of errors for all 200 dataset splits. The final model uses the modal
175 SEE but includes all data in the calibration dataset which, as it has more data, should result in a more
176 accurate model. Two hundred runs were chosen as this is the minimum number of runs where the SEE
177 range does not significantly increase, thus preserving computational cost while maintaining a
178 representative assessment. Natural data may vary from the calibration dataset and might not be

represented by an individual experiment. Therefore, we also use the IQR to calculate a confidence interval of the estimated value. We recommend users to use the and IQR double to the models SEE as a post-model filtering to remove poor estimates.

3. Results

3.1. Hyperparameter tuning

Hyperparameter tuning can help to achieve the best performing model possible (Breiman, 2002; Probst & Boulesteix, 2018). To systematically test the effect of hyperparameter variability, we ran 16,200 simulations which encompasses 81 combinations ranging from 1-9 `mtry` and 101-901 `ntrees` where each permutation is run 200 times with the respective test and train datasets to determine the average SEE and R^2, calculated using the ideal median pressures and temperatures.

The mean SEE varies with the number of trees (Figure 2) where the smaller number of trees performs marginally better than the larger number of trees (Figure 2b; for example, `mtry` = 2 the mean SEE for `ntree` varies from 4.63 to 4.59 kbar and 77.6 to 77.0 ºC from `ntree` 101 to 901). We suggest this is due to a plateau effect, as seen in other studies focused on hyperparameter tuning of random forests (Oshiro et al., 2012; Probst et al., 2019). Figure 2 (b, e) show a slight negative trend in both the pressure and temperature between 101 and 201 trees, but we stress that the difference is marginal. Clearly, we can see that the `mtry` has a larger control on the performance of the model, as expected from results in previous studies (Probst et al., 2019; Simm et al., 2014). As seen in Figure 2 (a, d), the larger `mtry` performs better (e.g., at `ntree` =201 an `mtry` of 6 gives a mean SEE of 4.37 kbar and 72.6 ºC) than the smaller `mtry` (e.g., at `ntree` =201 `mtry` of 1 give a mean SEE of 5.06 kbar and 84.5 ºC) for both the mean SEE and residuals. At `mtry` greater than 6, any difference is minor (± 0.01 kbar), and so to limit computational cost an `mtry` of 6 should be used. This is counter to the package default which is one third the number of total variables. A similar trend is observed in the calculated IQR. However, when considering data with the inclusion of liquid – crystal pairs, the new maximum `mtry` is 18 and hence a new `mtry` needs to be considered. We performed further testing on the model with the increased `mtry` and found that though the computational intensity increased the model follow

the same pattern as the models without liquid where the `ntree` is relatively invariable on the performance metrics and the `mtry` is optimized at about two thirds of the total variables (Supplementary Figure 2). As such, we suggest users select a `ntree` of 201 and an `mtry` equal to two thirds of the total variables for thermobarometry.

The package "`extraTrees`" also provides the option to vary the number of cuts at each node. This is easy to conceptualize in a classification model for grouping people on the basis of hair colour: instead of discriminating between black or blonde hair (binary choice), brown hair and red hair can also be considered as additional options (4 cuts). Whilst the default is 1 cut (binary), increasing the number of cuts to 3 – 5 may yield performance improvements (Simm & Magrans de Abril, 2013). Upon further testing we found that the additional number of cuts does minorly improve the model. However, the minor improvements to the SEE are less than 0.02 kbar and 0.5 ºC and so are not worth the significant increases in computational cost. Therefore, we continue to use the default of 1.

3.2. Mean, mode and median estimates

As discussed previously, the random forest is comprised of several hundred decision trees, as defined by the user via the function argument `ntree`. For each inputted sample `ntree` estimates for pressure and temperature are generated (Supplementary figure 3), and the final value is chosen from this distribution. The default option of the R package "`extraTrees`" in regression is for the forest to choose the mean of all decision tree outputs as the pressure or temperature (Simm et al., 2014). However, the distribution of the decision trees may not be a perfect gaussian distribution and thus we have also considered the median and modal estimates of the pressure and temperature voting distributions in addition to the mean (Figure 3).

To evaluate the performance of the mean, median, and modal estimates, we create pressure and temperature models using the entire calibration dataset for clinopyroxene, with no additional pressure filtering. The entire dataset is used instead of the 200 splits as a model with the full dataset included should perform the best and thus give the best estimates. Figure 3 shows estimated pressure plotted with respect to the true pressures for all 200 test datasets, using the mean, median, and modal method. The

residuals, the difference between the estimated and true pressure and temperature estimates, show the widest distribution of residuals for the mean and extend out to ±5 kbar. This means that many of the pressure estimates are incorrect by 5 kbar, indicating a poorly performing model. When we consider the SEE the median outcompetes both the mean and mode (median SEE = 3.27 kbar, mean SEE = 3.30 kbar, and mode SEE = 3.70 kbar). R^2 shows best performance from the mean (R^2 = 0.889) where the median (R^2 = 0.888) is slightly worse and the modal R^2 is also slightly worse (R^2 = 0.858).

3.3. Inclusion of equilibrium liquids

The elements that can be added to the structure of the clinopyroxene crystal is not just pressure and temperature dependent but also dependent to a certain degree on chemical availability in the residual liquid (melt). Thus, it is clear there needs to be two models – one with clinopyroxene data, as we have presented thus far, and one which also includes liquid data in equilibrium with the clinopyroxene. Performance testing of the two models (Figure 4) reveals that, as expected, the model performs more favourably when liquid data is included. Figure 4 shows that liquid model curves have a higher point density at 0 for the residuals, and IQR ranges closer to 0. For pressure, the SEE decreases by over 1 kbar and the R^2 changes from 0.80 to 0.89. For temperature, the difference is even more striking where the SEE decreases by almost half from 76.0 ºC to 47.6 ºC and the R^2 improves from 0.85 to 0.94. Performance of the 200 splits of the test and train dataset can be seen in the supplementary materials and shows that the liquid estimates have a slight tendency to estimate higher pressures relative to the liquid free model.

4. Discussion

4.1. Mean, mode, and median: which to use?

Fundamentally, if the distribution of decision trees produces a perfect gaussian distribution, then using the mean is appropriate. However, the distribution is often not a perfect gaussian curve. Some voting distributions may be uniform in which the model has a low degree of certainty. Other voting distributions show sharp peaks at a given value followed by small, wide tails to low and/or high pressure. Such tails initiate on poorly behaving trees, leading to overestimates of pressure or temperature due to unfair weighting by the mean of the distribution. Poorly behaving trees can result

from elements being selected for decision tree nodes which do not have a strong relationship with the variation of clinopyroxene unit cell parameters: these features ultimately govern the relationship between pressure, temperature, and mineral chemistry (Nimis & Ulmer, 1998).

Mean, median and modal models all perform well, although clearly the residuals from the modal and median model are preferable to the mean (Figure 3D). Considering the R^2 of modal versus median model estimates, modal estimates (0.858) are lower than that of the median (0.888). Despite the modal model showing a marginally tighter distribution of residuals, it has a fundamental flaw which is shown in Figure 5. Here, 10% of the calibration dataset was randomly extracted and a pressure gap between 5 and 15 kbar was forced into the training dataset. When the testing set is run in this pressure gapped model it is clear that the mode cannot interpolate any points in this pressure gap. Conversely, the median and mean models can close this gap by averaging values. Of course, this is an exaggerated example but it will indeed happen on smaller scales as experiments are often lacking in intermediate values (Hirschmann et al., 2008). In nature mineral chemistry typically shows a mixture of punctuated and continuous variability (Armienti et al., 2007; Conticelli et al., 2010). Thus, we suggest that all users adopt a median value for the PT estimates.

4.2. Evaluating the estimation uncertainty

Throughout the course of this work, we have optimized each model to give the best representation of the true (experimental) pressure and temperature. Though we have tested and optimized each model, there remains datapoints with high residuals, giving a poor estimate relative to the true experimental value (e.g., Figure 3). With natural samples the true pressure or temperature value is unknown and, if they exist in natural datasets, these anomalous samples cannot be identified. Thus far, we have assessed the overall performance of the calibrated models by using a mean SEE for each model (Figure 2). However, this averaged SEE characterises the model's ability to predict an entire test dataset and so does not provide a unique representation of the uncertainty of any specific sample. To permit closer assessment of uncertainty, we use the interquartile range (IQR) of the voting distribution (Figure 5) to assign the confidence interval of individual natural samples. The premise is that, although certain individual trees may perform poorly (see Methods above), a model that performs well overall will result

in a high number of trees predicting a pressure or temperature close to the true value. This will manifest in a voting distribution that is tight, indicating that the model has a high degree of certainty in its prediction.

To understand why some samples yield high IQRs and some low we will once again turn to our test and train datasets to look at some examples of variations in IQR. In Figure 6 we see three examples of the pressure estimates provided by the 201 trees represented by a density curve. The solid black vertical line is the estimated pressure using the median method, the solid red vertical line is the true pressure, and the two black vertical dashed lines represent the IQR. In Figure 6a we see a standard IQR value, where the true (2.0 kbar) and estimated (1.7 kbar) pressures are relatively close and the IQR is a reasonable value (2.4 kbar). Figure 6b shows the ideal case where the IQR is too small to see on the plot, and the estimated and true pressures are identical (10.0 kbar). Figure 6c shows a sample with a large IQR (12.3 kbar) and different true (16.0 kbar) and estimated (19.1 kbar) pressure. In this last case we see that the true pressure is still plotting within the IQR, however we recommend users treat any data with an IQR higher than half the overall model SEE with a healthy amount of caution.

The user may either present their natural data with the IQR or use the IQR as a metric for post-estimate filtering. Figure 7 shows a single split of the test and train dataset. In (a) the data is shown with the IQR plotted as pseudo error bars in which almost all of the points within their IQR ranges lie on the 1:1 line. In (b) there is an example of the same dataset but filtered to remove datapoints with an IQR larger than 5 kbar. We observe that points qualitatively identified as outliers are removed, and the points which remain plot closer to the 1:1 line. The same principle can be applied to temperature estimates. This approach encourages users to carefully consider their own data, and how it may contribute to their individual geological story: points with a low IQR may be considered more robust and interpretations can be based on these points with greater confidence.

4.3. Pressure filtering

Experiments which are performed under pressurized conditions require complex machinery and sometimes large time commitments (Holloway & Wood, 2012; Kägi et al., 2005; Leinenweber et al., 2012). Thus, the suite of data in the calibration dataset is heavily skewed towards experiments

performed at lower pressures (≤ 2 kbar). This is especially true for experiments performed at 1 atm, which comprise 23% of the filtered calibration dataset. We had concerns that this might unevenly skew the barometer estimates to lower pressures. To test this, we ran several models: the base model (or "mantle model"; P ≤ 50 kbar) and the "crustal model" (P ≤ 15 kbar), as chosen for the crustal range on the basis of the average crustal thickness (Kopp et al., 2011; MacKenzie et al., 2008; Tewari et al., 2018). Finally, we ran these two models with 1 atm experiments included and excluded.

As seen in Figure 8 there is not a strong effect on the residuals for the four models in pressure or temperature space. However, there is a slight effect on the IQR, with the density curves of crustal models for both pressure and temperature showing a higher density of low IQR values than the mantle model (Figure 8). Considering this quantitatively, we can turn to the average R^2 and SEE values over the 200 test and train dataset splits. For the "mantle-1 atm" in model the SEE is 4.4 kbar and 72.6 ºC, and R^2 of 0.80 for pressure and 0.85 for temperature, whereas the "crustal-1 atm in" model gives a lower SEE of 4.1 kbar and 69.4 ºC and an R^2 of 0.81 for the pressure model and 0.87 for the temperature model. When we consider the 1 atm excluded models, the "mantle-1 atm out" model gives an SEE of 3.4 and 70.8 ºC and a R^2 of 0.73 for pressure and 0.79 for temperature and the crustal model shows a similar trend of a lower SEE 3.1 kbar and 65.4 ºC and R^2 of 0.72 for pressure and 0.83 for temperature.

Given this information we must also consider one of the most striking limitations of a random forest algorithm – that it cannot extrapolate data. Thus, even though the crustal model has shown slight advantages with respect to IQR, and average SEE if a user inputs natural data, that may include clinopyroxenes that have crystallized in the mantle, into a crustal model low-pressure estimates might be generated. As such, we suggest that users employ the mantle model with the 1 atm experiments included. This is even more critical for compositions where experimental data is less dense. Alternatively, the distribution code contains instructions for tailoring models to user requirements such as changing bounds of pressure for application to areas with thicker (continental) crust (Bloch et al., 2017).

4.4. Adding liquid data to the model

As demonstrated in Figure 4, adding equilibrium liquid data improves the model (SEE is lower by >1 kbar and >30 ºC), and so quantitatively it seems favourable to use liquid data if it is available to users. In nature, however, opportunities for reliable coexisting melt measurement may be rare. Melt inclusions have been shown to suffer from post-entrapment crystallization which alters the composition of the melt inclusion (Bucholz et al., 2013; Danyushevssky et al., 2002; Steele-macinnis et al., 2011) or precipitation of daughter minerals of the edges of the melt inclusions (Moore et al., 2018; Venugopal et al., 2020). Additionally, melt inclusions may be absent in crystals or overrepresented in core or rim domains due to favourable growth along cracked surfaces (Faure & Schiano, 2005) or during heating, dissolution, and reprecipitation (Cashman & Blundy, 2013; Edmonds et al., 2016; Nakamura & Shimakita, 1998). Measuring matrix glass as the mineral - liquid pair is the most common metric for clinopyroxene- liquid thermobarometry. This may generate a bias in P-T estimates towards the final equilibration conditions of the upper part of the magmatic system, which may explain the questionable consensus that magma chambers form dominantly at ~2 kbar (Higgins et al., 2021). By using single-phase thermobarometers the entire protracted history of the crystal can be measured, which can recover the full extent of crystallisation P-T in trans crustal magmatic systems (Annen et al., 2006; Christopher et al., 2015; Sparks et al., 2019). Regardless, the performance of the liquid model is clearly superior to the crystal only melt, so we suggest that users of the liquid model keep a detailed petrological record of melt inclusions including distribution in the crystal and occurrence of mineral precipitation at melt inclusion margins.

5. Code distribution and Usage

We believe that our methodology can be widely implemented within the volcanology and petrology community. With this in mind, we have created two versions of the models which we are fondly calling "Choose your own adventure" and the "Plug and play" model. Both versions are available on github as a comprehensive R script for download at https://github.com/corinjorgenson/RandomForest-cpx-thermobarometer and archived on Zenodo at https://zenodo.org/record/5179981#.YROqtYgzaUl (Jorgenson et al., 2021). In this section we will describe how to use each of the respective scripts. Users who are not familiar with R are directed to "YaRrr! The Pirate's Guide to R", where Chapter 2 has

365 instructions for installation (https://bookdown.org/ndphillips/YaRrr/installing-base-r-and-rstudio.html,
366 Phillips, 2017).

367 5.1. Data collection recommendations

368 The "Plug and Play" models are created using a defined set of major oxides which a user must have
369 in their data to use the model. The elements are SiO_2, TiO_2, Al_2O_3, Cr_2O_3, FeO, MgO, MnO, CaO,
370 and Na_2O for the clinopyroxene analysis and SiO_2, TiO_2, Al_2O_3, FeO, MgO, MnO, CaO, Na_2O and
371 K_2O for the liquid analysis. If users do not have these elements, then they must use the "Choose
372 your own adventure" and adjust what elements are used to make the model. Liquid analysis should
373 be in equilibrium with the clinopyroxene host and this the two measurements should be taken
374 relatively close together. We recommend users input their data into the .csv file "InputData" and
375 replace the data there with their own, while keeping the column headers. If a user does not have
376 liquid data then they can leave it blank or put zeros in place.

377 5.2. Choose your own adventure

378 This folder comprises seven separate R scripts which should be run in order. The folder also includes
379 the initial calibration dataset as a .csv file, an example natural dataset, and an R data file with oxide
380 weights titled `cpx_dat`, `YOUR_DATA`, and `OxiWeight.Rdata` respectively. A brief explanation of
381 usage can be found in a .txt file titled README. Here we will sequentially discuss the code for each
382 file. We recommend between running each script, the user clears the environment and reloads the
383 necessary files to preserve computer memory. Whilst running this code, users should keep a keen eye
384 on the console in case of any errors. If there are any errors we advise clearing the environment and re-
385 running the code.

386 1. Preprocessing – cpx thermobaro

387 This script is used for pre-processing of the calibration dataset (Supplementary Table 1). All mineral
388 data are recalculated according to their respective structural formula following the methodology of Deer
389 et al. (1997). This is output as a file called `raw.Rdata`. You do not need to change anything in this
390 sheet unless you change the calibration dataset (e.g., to add new experimental data from the scientific

literature). If the user decides to add new experiments to the calibration dataset it is imperative that they format the new data the same way that the calibration dataset is currently formatted.

2. Filtering – cpx thermobaro

This script is used for filtering of the calibration dataset, choices for filtration limits can be found in section 2.1. The user does not need to change anything in this script unless they desire alternative filtrations (i.e., specific compositional or pressure filters).

Data outputted from script 1 (called `raw`) should be reloaded into the environment. This file is renamed to `dat`, and an extra column called `Rm` is added to the data frame which will have wither a `Y` or `N`, which dictates if data should be filtered (Y) or not (N).

First, the sum of cations is calculated and samples with cations above 4.04 or below 3.96 should be filtered out. Next, we calculate a value `kd` which is added to the data frame. As outlined in section 2.1 the Kd represents the whether the clinopyroxene and liquid are in equilibrium on the basis on the Fe/Mg ratio. The third filtration is to remove samples from the calibration dataset above 50 kbars, as there is not sufficient data accurately estimate pressure at these pressures. Lastly, we filter for extremely low liquid SiO_2 contents, which we have set as 35 wt.% SiO_2.

The data is filtered so the samples which were assigned `Y` to the `Rm` column are removed. Then the calibration dataset is mixed to avoid bias in organization of the data. This filtered data frame is then called `input` and saved as an Rdata file.

3. Distribute Grid Search

This script and the next one (Determine SEE) are used to determine the SEE for the final models by extracting 200 test and training datasets and then running the model 200 times and calculating the SEE based on that. Section 2.3 explains further the idea behind extracting 200 splits. The user does not need to change anything in this script unless they want to change how many test/train splits there are.

In this script the calibration dataset is loaded in as `input.Rdata`. First, we decide of how many test/train datasets, which is controlled by the variable `r`. Then we extract the index places of the 200

testing datasets. The test dataset is ~10% depending on how many points are in the calibration dataset (`input`). In the `for` loop (which runs `r = 200`) times a grid system is defined where `P/T.upper/lower` are the bounds for each grid square. `perms` gives all the possible combinations for the lower P and T bounds, and then has the upper bounds added to it. `sam` is the actual grid, which is sampled in `samp`. `samp` sampled one sample from each of the grid squared and adds it to `perms`. From `perms`, we determine the number of points in each of the grid squares and the grid squares with less than two points are removed from the sampled point (`no.perms`). Finally, the samples from each of the grid squares (`perms`) are called `test.ids`. This is just the test data set, so the identities of the training dataset are determined as well and called `train.ids`. Both the `test.ids` and `train.ids` are saved as .Rdata files.

4. Determine SEE – cpx thermobaro

This code determines the average SEE for the P and T models. In this script the user can decide on whether they want to use liquid data or not. It is imperative that whatever conditions you use for this script are the same as script #5. We strongly recommend you clear the environment before using this script.

The calibration dataset is loaded into the environment as `input.Rdata` and the test and train ids are loaded as `testids.Rdata` and `trainids.Rdata`. Next, users can decide if they want to include liquid data in the model (`liq <- c("Liquid")`) or not (`liq <- c("NoLiquid")`). Next, elements that will go into the model are chosen, the order of these elements must be the same in this script as in script #5 or the model will read the wrong elements and return a very poor predictor. Elements for the clinopyroxene are defined in `ox` and for the liquid phase is in `liqox`. Next the `r` value (200, as in script #3) and hyperparameters are defined, we direct the reader to section 3.1 for further information on these. Lastly, if you wish to filter any pressure you can here (1 atm experiments included or excluded). The calibration dataset at this stage is renamed `dat` for the rest of the script.

Objects `id.test` and `id.train` are used determine the ids of the test/train sets in the `dat` (calibration dataset) data frame. A set of empty lists are made for the data to be filled into. The `for`

loop is run `r` (200) times. For each run, the training set is used to create the model and the test set is inputted into the model and pressures are estimated using the median pressure determination. From this estimated pressure the residuals, R^2 and SEE are calculated. This is done for both pressure and temperature and loaded into output, which is reduced and saved as `final.Rdata`. From these 200 run the average SEE can be determined by calculating the average SEE. This code is the longest computational time, while it is running you should see `j` printed in the console twice (up to 200 times, once for pressure and once for temperature) to keep you updated on where you are in the model.

This calculates the mean, median, and modal pressures, as discussed above we suggest that users use the median estimates moving forward, but as this version is choose you own adventure we leave this option up to the user. If you choose to rune this script several times you may notice minor differences in the SEE (~ 0.2 kbar and ~10 ºC). These variations are a fundamental part of the random forest, that it is random!

5. Final Model Training – cpx thermobaro

This script has the SEE as calculated in script #4 and thus any changes made in script #4 must be made in this script as well, the options are the same as script #4. This script makes the actual model. Once you have made and saved this model you can continue to use this model in script 6 for any datasets you desire without needing to re-run scripts 1-5 for the calibration dataset. The models are called `P_C` and `T_C` for the pressure and temperature models respectively and saved as. Rdata files.

6. Filter user data – cpx thermobaro

This script is essentially the same as script #1 and #2 with some adjustments to avoid overwriting the calibration dataset or your data. User's will need to change the code `userdat <- read.delim("InputData.txt")` to reflect the title of their data or copy and paste your data into the InputData.csv file (and remove the data we have there) so the formatting is correct. Else, make sure your cations are properly suffixed (.cpx for clinopyroxene and .liq for the liquid data).

7. Run the model – cpx thermobaro

This script this the final step, where you can input your data and get pressure and temperature estimates! You inputted data should be filtered as in script #6. The models are loaded in as `P_C.Rdata` and `T_C.Rdata` and outputted as `predP` and `predT` respectively. Your data is loaded in and subsetted for the elements used to make the model. Once again it is imperative that the element order is the same or the outputs will be wrong.

The code then takes the `pred P` and `predT` and calculates the respective mean, median, mode, and IQR estimates using the apply function. After the colon of each line the data is saved the `OUTPUTDATA` dataframe. This `OutputData.csv` is the final file with your estimated values!

5.3. Plug and play

This script and corresponding .Rdata files allow the user to use a pre-determined model with a pre-set SEE for either liquid or no liquid data. These models are run with `ntree =201, mtry =6, numcuts =1`, pressures input from 0-50 kbar (with 1 atm included). The SEE for the liquid model is 3.2 kbar, 47.6 ºC and for the no liquid models SEE of 4.4 kbar and 76.0 º C.

This model assumes that the user has already filtered their data for poor totals. Users are requested to copy and paste their data into the example excel file InpudtData.csv and leave the column headers so the suffixes are saved. Clinopyroxene major oxides should be the same as in the model and need to be suffixed with .cpx even if using a no liquid model and liquid/melt analysis should be suffixed with .liq. Examples and lists of the major oxides needed are in the script itself.

To use the script users will need to first open R studio and comment (add a #) and uncomment (remove #) to be reflective if they have liquid data or not. For example if you aren't using liquid data then the code should look like:

```
liq <- "NoLiquid"

# liq <- "Liquid"
```

And if you do have liquid data the # will be in front of the first line and not in front of the second line. After this step the user should be able to select all the code and press run. Your data is saved as a csv called `OutputData.csv`. The end of the script features some basic plots you can use with your data, though we encourage user to delve into the wonderful world of plotting in R for themselves.

6. Conclusions

We have shown that machine learning is a powerful and versatile approach to thermobarometry, in agreement with other studies (Higgins et al., 2021; Petrelli et al., 2020). Through detailed testing we have determined that our models have accuracy and precision comparable to the leading clinopyroxene thermobarometers (Masotta et al., 2013; Neave & Putirka, 2017; K. D. Putirka, 2008). This thermobarometer can be applied to a wider range of compositions with a similar performance as existing models. Additionally, this model as has the added benefit of error estimates on individual estimates, where users can discard poorly performing estimates if they desire. Hyperparameters generally make little difference to the performance of the thermobarometer. The largest effect is the value of `mtry` which, at low values (1 or 2), creates a more poorly performing model (Figure 2). Instead, the largest effect on model performance is the method of output determination i.e., whether the mean, median, or mode of the voting distribution is used to recover pressure and temperature. Here we reveal that, although the mean can provide reasonable pressure and temperature estimates, cases where there are poorly performing trees may yield anomalously high-pressure predictions for low-pressure experiments. The mode, on the other hand, seems to give values with the lowest residuals but struggles to reproduce data reliably in significant pressure and temperature gaps (Figure 5a). Thus, we recommend a semi-automated approach where users filter their data using the interquartile range of the voting distribution but rely on the median value of the predicted pressure and temperature. This allows for consistently lower residual values when predicting experimental data.

Two sets of codes have been created, with detailed comments and instructions, for the Earth sciences community to rapidly predict intensive parameters for natural data, or create more tailored models. The purpose of this paper is to provide a framework for use of machine learning thermobarometry in Earth Sciences for users of widely differing computing experience. We believe that our model, given the right

considerations, can result in a high-resolution study of crustal magmatic systems. Future work will focus on testing the model with chemically independent pressure and temperature estimates and show examples of how this model can be utilized for different melt compositions.

7. Acknowledgments

We would also like to thank all the experimental petrologist whose hours of work make this model possible whose data is available at http://lepr.ofm-research.org/YUI/access_user/login.php. OH and LC received funding from the European Research Council (ERC) under the European Union's Horizon 2020 research and innovation program (Grant agreement 677493 -FEVER). CJ and LC received funding from the Swiss National Science 454 Foundation (grant n. 200021_184632). MP received funding from the Università degli Studi di Perugia "ENGAGE" FRB-2019 grant.

Version 1.0 of the software Random Forest cpx-thermobarometer is preserved at DOI:10.5281/zenodo.5179981, https://zenodo.org/record/5179981#.YRPif4gzY2w and is available via creative commons attribution. Subsequent versions of the code are available at https://github.com/corinjorgenson/RandomForest-cpx-thermobarometer.

8. References

Annen, C., Blundy, J. D., & Sparks, R. S. J. (2006). The genesis of intermediate and silicic magmas in deep crustal hot zones. *Journal of Petrology*, *47*(3), 505–539. https://doi.org/10.1093/petrology/egi084

Armienti, P., Tonarini, S., Innocenti, F., & D'Orazio, M. (2007). Mount Etna pyroxene as tracer of petrogenetic processes and dynamics of the feeding system. *Special Paper of the Geological Society of America*, *418*(January 2007), 265–276. https://doi.org/10.1130/2007.2418(13)

Bloch, E., Ibañez-Mejia, M., Murray, K., Vervoort, J., & Müntener, O. (2017). Recent crustal foundering in the Northern Volcanic Zone of the Andean arc: Petrological insights from the roots of a modern subduction zone. *Earth and Planetary Science Letters*, *476*, 47–58. https://doi.org/10.1016/j.epsl.2017.07.041

Breiman, L. (2001). Random forests. *Machine Learning*, *45*, 5–32. https://doi.org/10.1201/9780367816377-11

Breiman, L. (2002). Manual on Setting Up, Using, and Understanding Random Foest V3.1. *Statistics Department University of California Berkeley, CA, USA*, *1*(58).

547 Bucholz, C. E., Gaetani, G. A., Behn, M. D., & Shimizu, N. (2013). Post-entrapment modification of
548 volatiles and oxygen fugacity in olivine-hosted melt inclusions. *Earth and Planetary Science*
549 *Letters*, *374*, 145–155. https://doi.org/10.1016/j.epsl.2013.05.033
550 Cashman, K., & Blundy, J. (2013). Petrological cannibalism: The chemical and textural consequences
551 of incremental magma body growth. *Contributions to Mineralogy and Petrology*, *166*(3), 703–
552 729. https://doi.org/10.1007/s00410-013-0895-0
553 Christopher, T., Blundy, J., Cashman, K., Cole, P., Edmonds, M., Smith, P., Sparks, R. S. J., &
554 Stinton, A. (2015). Geochemistry, Geophysics, Geosystems. *Geochemistry Geophysics*
555 *Geosystems*, *18*(1–2), 1541–1576. https://doi.org/10.1002/2015GC005791.Received
556 Conticelli, S., Boari, E., & Avanzinelli, R. (2010). *The Colli Albani Volcano: Speical Publications of*
557 *IAVCEI* (Issue 3).
558 Danyushevsky, L. V., McNeill, A. W., & Sobolev, A. V. (2002). Experimental and petrological
559 studies of melt inclusions in phenocrysts from mantle-derived magmas: An overview of
560 techniques, advantages and complications. *Chemical Geology*, *183*(1–4), 5–24.
561 https://doi.org/10.1016/S0009-2541(01)00369-2
562 Deer, W. A., Howie, R. A., & Zussman, J. (1997). *Rock-forming minerals: single-chain silicates*
563 (Volume 2A). Geological Society of London.
564 Edmonds, M., Kohn, S. C., Hauri, E. H., Humphreys, M. C. S., & Cassidy, M. (2016). Extensive,
565 water-rich magma reservoir beneath southern Montserrat. *Lithos*, *252–253*, 216–233.
566 https://doi.org/10.1016/j.lithos.2016.02.026
567 Faure, F., & Schiano, P. (2005). Experimental investigation of equilibration conditions during
568 forsterite growth and melt inclusion formation. *Earth and Planetary Science Letters*, *236*(3–4),
569 882–898. https://doi.org/10.1016/j.epsl.2005.04.050
570 Georgeais, G., Koga, K. T., Moussallam, Y., & Rose-Koga, E. F. (2021). Magma decompression rate
571 calculations with EMBER: A user-friendly software to model diffusion of H 2 O, CO 2 and S in
572 melt embayments . *Geochemistry, Geophysics, Geosystems*.
573 https://doi.org/10.1029/2020gc009542
574 Ghiorso, M. S., & Wolf, A. . (2019). *Thermodynamic Modeling Using ENKI: 1. Overview and Phase*

Equilibrium Applications.

Giacomoni, P. P., Coltorti, M., Bryce, J. G., Fahnestock, M. F., & Guitreau, M. (2016). Mt . Etna plumbing system revealed by combined textural , compositional , and thermobarometric studies in clinopyroxenes. *Contributions to Mineralogy and Petrology*, *171*(4), 1–15. https://doi.org/10.1007/s00410-016-1247-7

Higgins, O., Sheldrake, T., & Caricchi, L. (2021). Machine learning thermobarometry and chemometry using amphibole and clinopyroxene : a window into the roots of an arc volcano (Mount Liamuiga , Saint Kitts). *EarthArXiv*.

Hirschmann, M. M., Ghiorso, M. S., Davis, F. A., Gordon, S. M., Mukherjee, S., Grove, T. L., Krawczynski, M., . Medard, E., & Till, C. B. (2008). Library of Experimental Phase Relations (LEPR): A database and Web portal for experimental magmatic phase equilibria data. *Geochemistry, Geophysics, Geosystems*, *9*(3). https://doi.org/10.1029/2007GC001894

Ho, T. K. (1995). Random decision forests. *Proceedings of the International Conference on Document Analysis and Recognition, ICDAR*, *1*, 278–282. https://doi.org/10.1109/ICDAR.1995.598994

Holloway, J. R., & Wood, B. J. (2012). *Simulating the Earth: experimental geochemisty*. Springer Science & Business.

Iacovino, K., Matthews, S., Wieser, P. E., Moore, G. M., & Bégué, F. (2020). *VESIcal Part I : An open-source thermodynamic model engine for mixed volatile (H2O-CO2) solubility in silicate melts*. 1–58.

Jorgenson, C., Higgins, O., Petrelli, M., Bégué, F., & Caricchi, L. (2021). *RandomForest-cpx-thermobarometer code* (v1.0). Zenodo. https://doi.org/10.5281/zenodo.5179981

Kägi, R., Müntener, O., Ulmer, P., & Ottolini, L. (2005). Piston-cylinder experiments on H2O undersaturated Fe-bearing systems: An experimental setup approaching fO2 conditions of natural calc-alkaline magmas. *American Mineralogist*, *90*(4), 708–717. https://doi.org/10.2138/am.2005.1663

Klügel, A., & Klein, F. (2006). Complex magma storage and ascent at embryonic submarine volcanoes from the Madeira Archipelago. *Geology*, *34*(5), 337.

https://doi.org/10.1130/G22077.1

Kopp, H., Weinzierl, W., Becel, A., Charvis, P., Evain, M., Flueh, E. R., Gailler, A., Galve, A., Hirn, A., Kandilarov, A., Klaeschen, D., Laigle, M., Papenberg, C., Planert, L., & Roux, E. (2011). Deep structure of the central Lesser Antilles Island Arc: Relevance for the formation of continental crust. *Earth and Planetary Science Letters*, *304*(1–2), 121–134. https://doi.org/10.1016/j.epsl.2011.01.024

Leinenweber, K. D., Tyburczy, J. A., Sharp, T. G., Soignard, E., Diedrich, T., Petuskey, W. B., Wang, Y., & Mosenfelder, J. L. (2012). Cell assemblies for reproducible multi-anvil experiments (the COMPRES assemblies). *American Mineralogist*, *97*(2–3), 353–368. https://doi.org/10.2138/am.2012.3844

Lemenkova, P. (2019). An empirical study of R applications for data analysis in marine geology. *Marine Science and Technology Bulletin*, *8*, 1–9. https://doi.org/10.33714/masteb.486678

Lubbers, J., Kent, A. J. R., Meisenheimer, D. E., & Wildenschild, D. (2019). *Using MicroCT to Quantify 3D Zoning in Sanidine: Implications for Magma Reservoir Processes*.

MacKenzie, L., Abers, G. A., Fischer, K. M., Syracuse, E. M., Protti, J. M., Gonzalez, V., & Strauch, W. (2008). Crustal structure along the southern Central American volcanic front. *Geochemistry, Geophysics, Geosystems*, *9*(8). https://doi.org/10.1029/2008GC001991

Masotta, M., Mollo, S., Freda, C., Gaeta, M., & Moore, G. (2013). Clinopyroxene–liquid thermometers and barometers specific to alkaline differentiated magmas. *Contributions to Mineralogy and Petrology*, *166*(6), 1545–1561. https://doi.org/10.1007/s00410-013-0927-9

Moore, L. R., Mironov, N., Portnyagin, M., Gazel, E., & Bodnar, R. J. (2018). Volatile contents of primitive bubble-bearing melt inclusions from Klyuchevskoy volcano, Kamchatka: Comparison of volatile contents determined by mass-balance versus experimental homogenization. *Journal of Volcanology and Geothermal Research*, *358*, 124–131. https://doi.org/10.1016/j.jvolgeores.2018.03.007

Nakamura, M., & Shimakita, S. (1998). Dissolution origin and syn-entrapment compositional change of melt inclusion in plagioclase. *Earth and Planetary Science Letters*, *161*(1–4), 119–133. https://doi.org/10.1016/S0012-821X(98)00144-7

631 Neave, D. A., & Putirka, K. D. (2017). A new clinopyroxene-liquid barometer, and implications for
632 magma storage pressures under Icelandic rift zones. *American Mineralogist*, *102*(4), 777–794.
633 https://doi.org/10.2138/am-2017-5968
634 Nimis, P., & Taylor, W. R. (2000). Single clinopyroxene thermobarometry for garnet peridotites. Part
635 I. Calibration and testing of a Cr-in-Cpx barometer and an enstatite-in-Cpx thermometer.
636 *Contributions to Mineralogy and Petrology*, *139*(5), 541–554.
637 https://doi.org/10.1007/s004100000156
638 Nimis, P., & Ulmer, P. (1998). Clinopyroxene geobarometry of magmatic rocks. Part 1: An expanded
639 structural geobarometer for anhydrous and hydrous, basic and ultrabasic systems. *Contributions*
640 *to Mineralogy and Petrology*, *133*(1–2), 122–135. https://doi.org/10.1007/s004100050442
641 Oshiro, T. M., Perez, P. S., & Baranauskas, J. A. (2012). How many trees in a random forest? *Lecture*
642 *Notes in Computer Science (Including Subseries Lecture Notes in Artificial Intelligence and*
643 *Lecture Notes in Bioinformatics)*, *7376 LNAI*, 154–168. https://doi.org/10.1007/978-3-642-
644 31537-4_13
645 Petrelli, M., Caricchi, L., & Perugini, D. (2020). Machine Learning Thermo-barometry: Application
646 to clinopyroxene bearing magma, In Review. *Submitted to JGR: Solid Earth*, *3*(2), 54–67.
647 http://repositorio.unan.edu.ni/2986/1/5624.pdf
648 Phillips, N. D. (2017). *YaRrr! The Pirate's Guide to R*.
649 Probst, P., & Boulesteix, A. L. (2018). To tune or not to tune the number of trees in random forest.
650 *Journal of Machine Learning Research*, *18*, 1–8.
651 Probst, P., Wright, M. N., & Boulesteix, A. L. (2019). Hyperparameters and tuning strategies for
652 random forest. *Wiley Interdisciplinary Reviews: Data Mining and Knowledge Discovery*, *9*(3),
653 1–15. https://doi.org/10.1002/widm.1301
654 Putirka, K. (1999). Clinopyroxene + liquid equilibria to 100 kbar and 2450 K. *Contributions to*
655 *Mineralogy and Petrology*, *135*(2–3), 151–163. https://doi.org/10.1007/s004100050503
656 Putirka, K. D. (2008). Thermometers and barometers for volcanic systems. *Reviews in Mineralogy*
657 *and Geochemistry*, *69*, 61–120. https://doi.org/10.2138/rmg.2008.69.3
658 Ridolfi, F., Puerini, M., Renzulli, A., Menna, M., & Toulkeridis, L. (2008). *The magmatic feeding*

659 *system of El Reventador volcano (Sub-Andean zone , Ecuador) constrained by texture ,*
660 *mineralogy and thermobarometry of the 2002 erupted products*. *176*, 94–106.
661 https://doi.org/10.1016/j.jvolgeores.2008.03.003
662 Ridolfi, F., & Renzulli, A. (2012). Calcic amphiboles in calc-alkaline and alkaline magmas:
663 Thermobarometric and chemometric empirical equations valid up to 1,130°C and 2.2 GPa.
664 *Contributions to Mineralogy and Petrology*, *163*(5), 877–895. https://doi.org/10.1007/s00410-
665 011-0704-6
666 Ridolfi, F., Renzulli, A., & Puerini, M. (2010). Stability and chemical equilibrium of amphibole in
667 calc-alkaline magmas: An overview, new thermobarometric formulations and application to
668 subduction-related volcanoes. *Contributions to Mineralogy and Petrology*, *160*(1), 45–66.
669 https://doi.org/10.1007/s00410-009-0465-7
670 Shane, P., & Smith, V. C. (2013). Lithos Using amphibole crystals to reconstruct magma storage
671 temperatures and pressures for the post-caldera collapse volcanism at Okataina volcano
672 Haroharo Haroharo caldera Rotoiti collapse Tarawera. *LITHOS*, *156–159*, 159–170.
673 https://doi.org/10.1016/j.lithos.2012.11.008
674 Shaw, C. S. J. (2018). Lithos Evidence for the presence of carbonate melt during the formation of
675 cumulates in the Colli Albani Volcanic District , Italy. *LITHOS*, *310–311*, 105–119.
676 https://doi.org/10.1016/j.lithos.2018.04.007
677 Simm, J., & Magrans de Abril, I. (2013). Package for ExtraTrees method for classification and
678 regression. *IEICE TRANSACTIONS on Information and Systems*, 3–5.
679 Simm, J., Magrans De Abril, I., & Sugiyama, M. (2014). Tree-based ensemble multi-task learning
680 method for classification and regression. *IEICE Transactions on Information and Systems*, *E97-*
681 *D*(6), 1677–1681. https://doi.org/10.1587/transinf.E97.D.1677
682 Smith, D. (2013). *Olivine thermometry and source constraints for mantle fragments in the Navajo*
683 *Volcanic Field, Colorado Plateau, southwest United States: Implications for the mantle wedge*.
684 *14*(3), 693–711. https://doi.org/10.1002/ggge.20065
685 Sparks, R. S. J., Annen, C., Blundy, J. D., Cashman, K. V., Rust, A. C., & Jackson, M. D. (2019).
686 Formation and dynamics of magma reservoirs. *Philosophical Transactions of the Royal Society*

A: Mathematical, Physical and Engineering Sciences, *377*(2139). https://doi.org/10.1098/rsta.2018.0019

Steele-macinnis, M., Esposito, R., & Bodnar, R. J. (2011). Thermodynamic model for the effect of post-entrapment crystallization on the H 2 O-CO 2 systematics of vapor-saturated, silicate melt inclusions. *Journal of Petrology*, *52*(12), 2461–2482. https://doi.org/10.1093/petrology/egr052

Tewari, H. C., Rajendra Prasad, B., & Kumar, P. (2018). Global and Indian Scenario of Crustal Thickness. In *Structure and Tectonics of the Indian Continental Crust and Its Adjoining Region* (2nd ed.). Elsevier Inc. https://doi.org/10.1016/b978-0-12-813685-0.00009-1

Venugopal, S., Schiavi, F., Moune, S., Bolfan-Casanova, N., Druitt, T., & Williams-Jones, G. (2020). Melt inclusion vapour bubbles: the hidden reservoir for major and volatile elements. *Scientific Reports*, *10*(1), 1–14. https://doi.org/10.1038/s41598-020-65226-3

Ziberna, L., Nimis, P., Kuzmin, D., & Malkovets, V. G. (2016). Error sources in single-clinopyroxene thermobarometry and a mantle geotherm for the Novinka kimberlite, Yakutia. *American Mineralogist*, *101*(10), 2222–2232. https://doi.org/10.2138/am-2016-5540

9. Figures

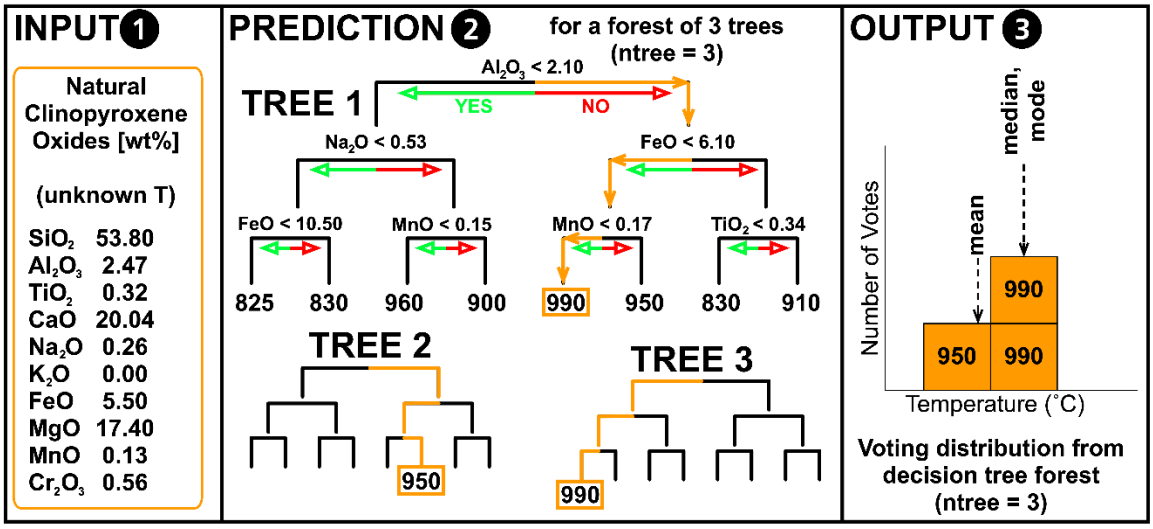

Figure 1. Process of determining temperature from a natural (unknown T) clinopyroxene using machine learning thermobarometry. The input to the model (1) is the chemistry of the natural clinopyroxene. The chemical composition is cascaded through each decision tree in turn (2; orange path), arriving at the temperature at the base of each tree. The voting distribution (3; output) is used to determine the temperature. This temperature can be selected based on the mean, median or mode of the voting distribution (see text for details)

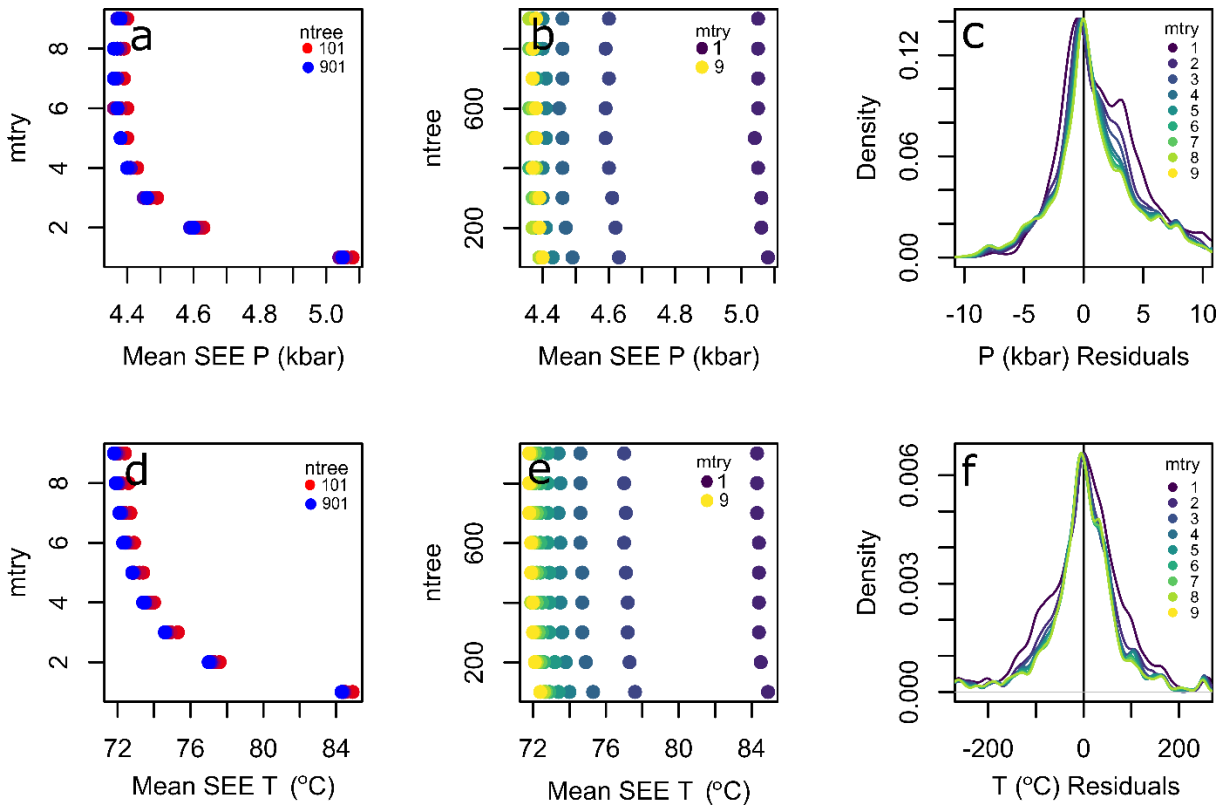

710

711 *Figure 2. Distribution of the* `mtry` *(a and d),* `ntree` *(b and e), and residuals (c and f) for both*

712 *pressure and temperatures calculated using the modal method. Each point represents the average SEE*

713 *for each of the 200 runs for each* `mtry` *and* `ntree` *combination. The residual plots are density plots*

714 *of the residuals from the 200 run for* `mtry` *values from 1 to 9, at a constant* `ntree` *of 201*

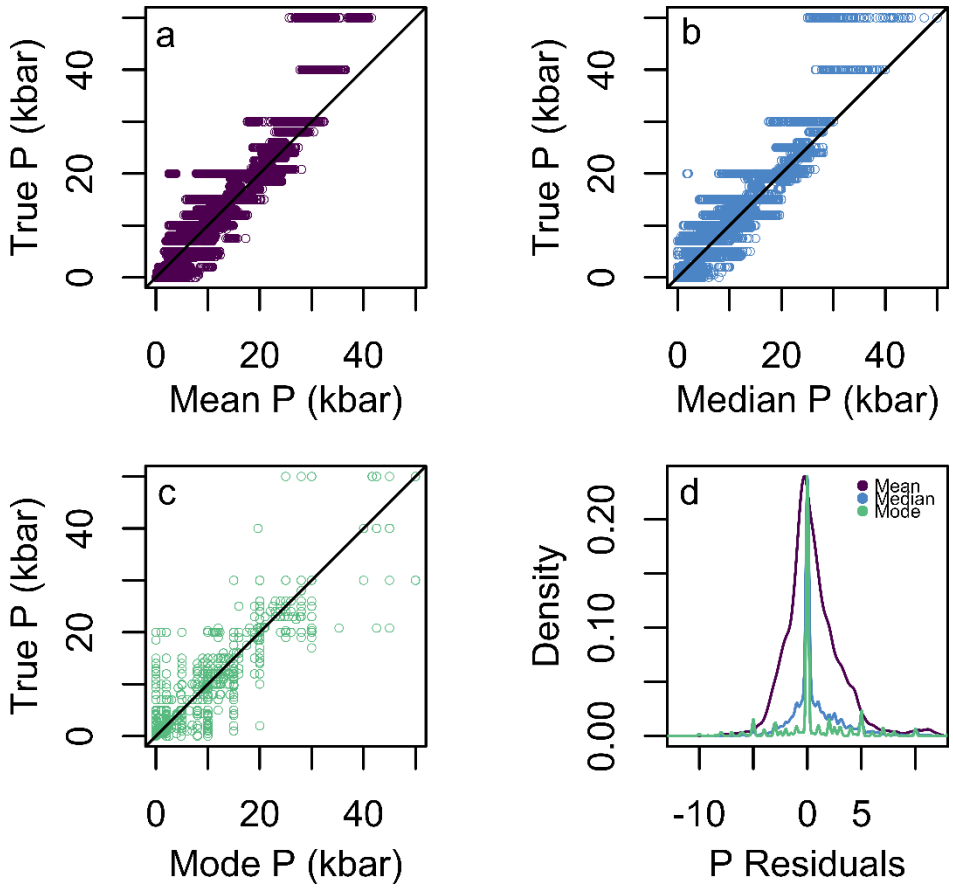

715

716 *Figure 3. Mean (SEE = 3.3 kbar, R^2 = 0.889) (a), median (SEE = 3.3 kbar, R^2 = 0.888) (b), and modal*

717 *(SEE = 3.7 kbar, R^2 = 0.858) (c) pressure determinations for the 200 test datasets versus their true*

718 *pressure. d) Density plots of the residuals for the mean, median, and mode.*

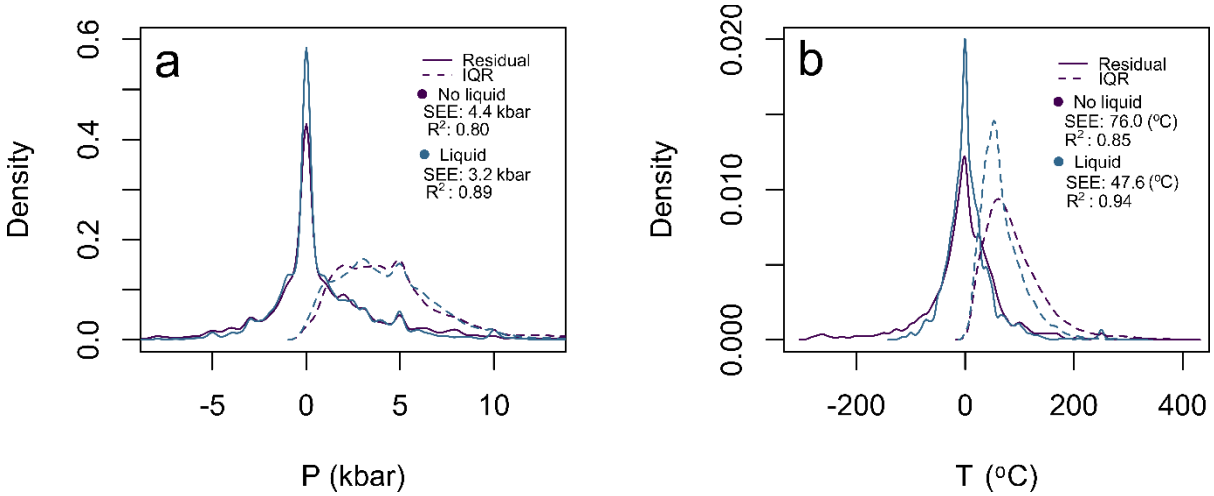

719

720 *Figure 4. Residuals (solid) and IQR (dashed) density plots for liquid and no liquid models, plots are*

721 *for pressure (a) and temperature (b)*

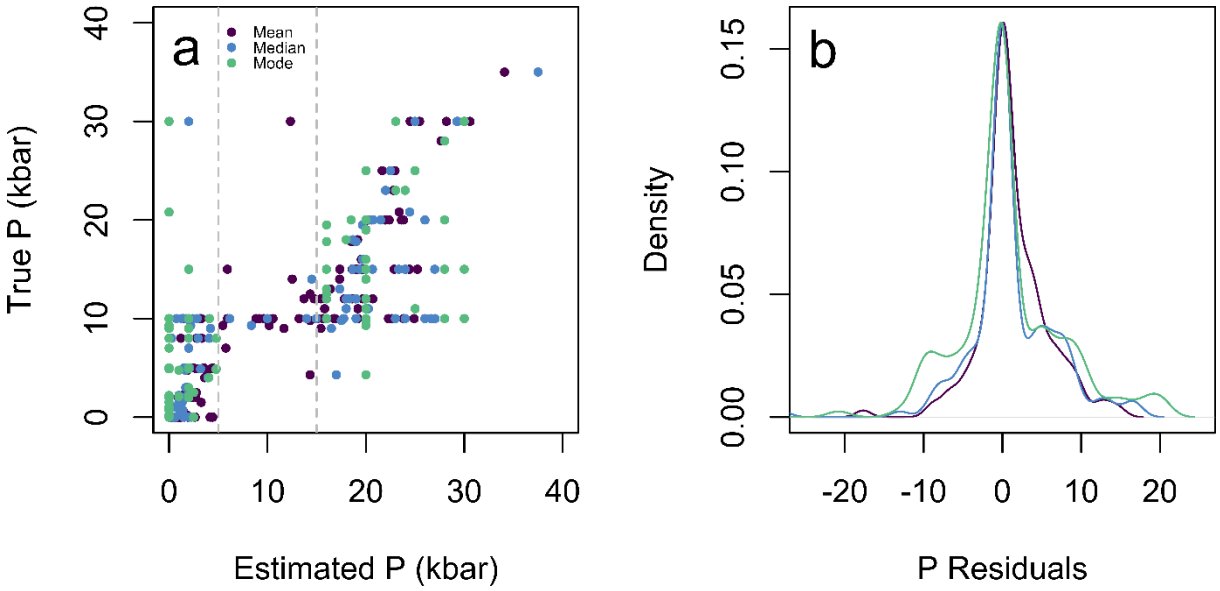

Figure 5. Results from a model with a pressure gap from 5 to 15 kbar forced into the calibration dataset (grey dashed lines). Clearly seen in a and b is the poor performance of the modal estimates

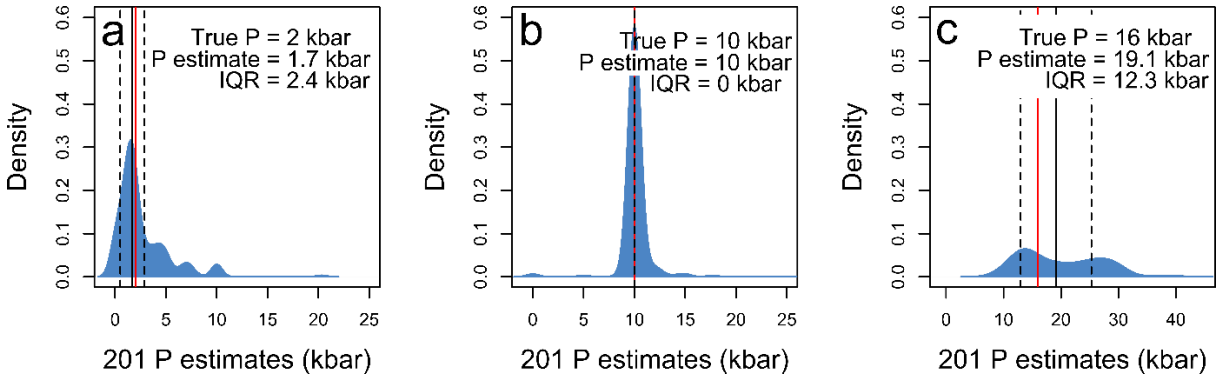

Figure 6. Figure explaining the components of the IQR and showing examples of samples which have generated a high (c) and low (b) IQR. Samples plotted here are the 201 estimates given from one forest for one sample. The solid black vertical line is the estimated pressure using the median method, the solid red vertical line is the true pressure, and the two black vertical dashed lines represent the IQR. Text on the plot shows the true pressure, estimated pressure and interquartile range, all in kbar.

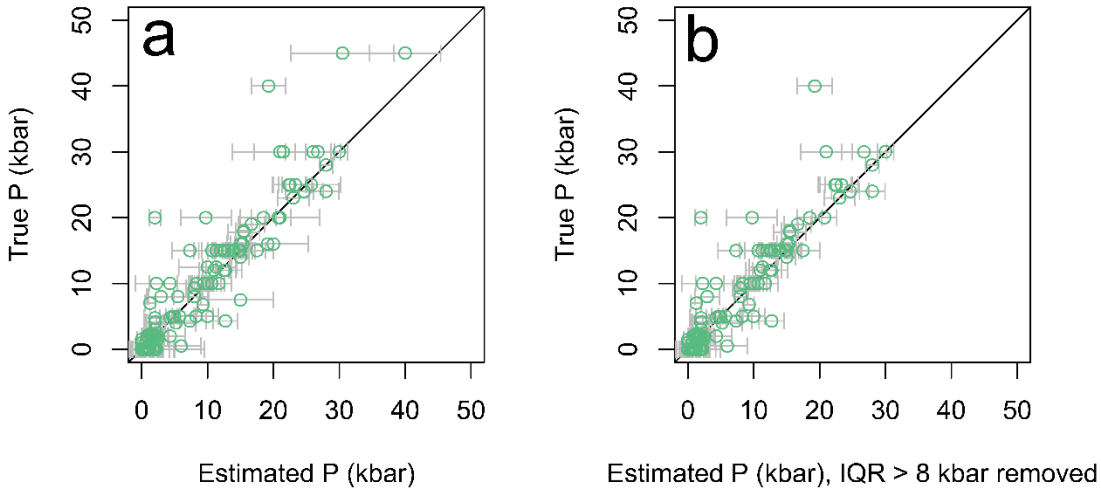

732

733 *Figure 7. a) Single split of the test/train dataset plotted with the IQR as one would with error bars in*

734 *grey. b) the same dataset but filtered to remove IQR larger than 8 kbar*

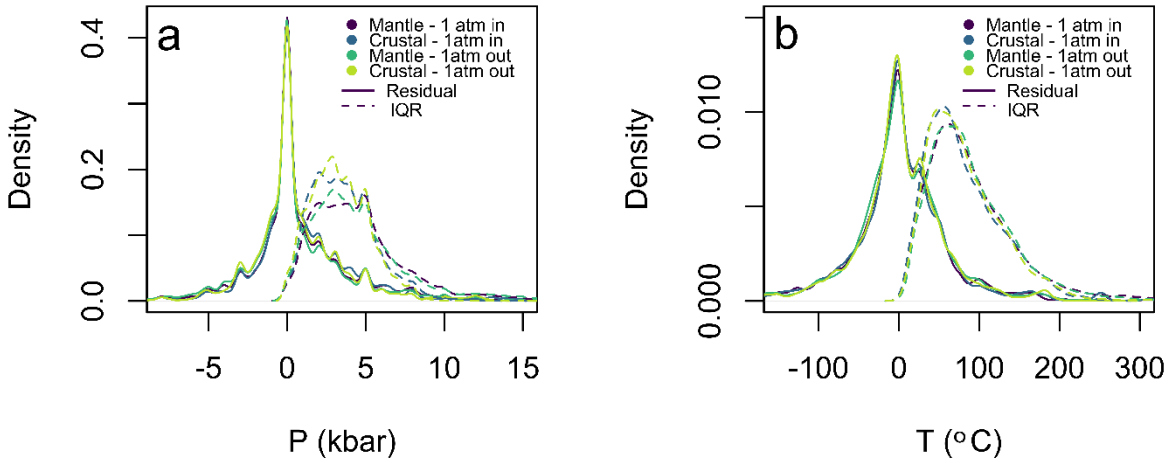

735

736 *Figure 8. Residuals (solid) and IQR (dashed) density plots for the pressure filtered models mantle (0-*

737 *70 kbar), crustal (0-15 kbar) with and without the 1 atm experiments. Plots are for pressure (a) and*

738 *temperature (b)*

739